Front. Struct. Civ. Eng. 2019, 13(5): 1271–1287
https://doi.org/10.1007/s11709-019-0556-0

RESEARCH ARTICLE

Experimental study on flexural behavior of ECC/RC composite beams with U-shaped ECC permanent formwork

Zhi QIAO[a], Zuanfeng PAN[a,b*], Weichen XUE[b], Shaoping MENG[c]

[a] *Key Laboratory of Concrete & Prestressed Concrete Structures of the Ministry of Education, Southeast University, Nanjing 210096, China*

[b] *College of Civil Engineering, Tongji University, Shanghai 200092, China*

[c] *School of Civil Engineering, Southeast University, Nanjing 210096, China*

[*] *Corresponding author. E-mail: zfpan@tongji.edu.cn*

ABSTRACT To enhance the durability of a reinforced concrete structure, engineered cementitious composite (ECC), which exhibits high tensile ductility and good crack control ability, is considered a promising alternative to conventional concrete. However, broad application of ECC is hindered by its high cost. This paper presents a new means to address this issue by introducing a composite beam with a U-shaped ECC permanent formwork and infill concrete. The flexural performance of the ECC/RC composite beam has been investigated experimentally with eight specimens. According to the test results, the failure of a composite beam with a U-shaped ECC formwork is initiated by the crushing of compressive concrete rather than debonding, even if the surface between the ECC and the concrete is smooth as-finished. Under the same reinforcement configurations, ECC/RC composite beams exhibit increases in flexural performance in terms of ductility, load-carrying capacity, and damage tolerance compared with the counterpart ordinary RC beam. Furthermore, a theoretical model based on the strip method is proposed to predict the moment-curvature responses of ECC/RC composite beams, and a simplified method based on the equivalent rectangular stress distribution approach has also evolved. The theoretical results are found to be in good agreement with the test data.

KEYWORDS engineered cementitious composite (ECC), durability, ECC/RC composite beam, permanent formwork, flexural performance, theoretical method

1 Introduction

Concrete is usually subjected to tensile stresses due to loading, processing, shrinkage, and thermal effects. The brittleness of concrete in tension essentially leads to the formation of cracks, which is of special concern in structures with respect to durability. Unfortunately, the crack width of concrete increases linearly with applied load [1]. Wider cracks increase the migration of aggressive agents into concrete, leading to severe reinforcement corrosion, spalling, strength loss, or progressive disintegration. Hence, it is important to control the width of cracks in reinforced concrete (RC) structures.

Article history: Received Oct 5, 2018; Accepted Dec 21, 2018

In recent years, efforts to modify the brittle nature of ordinary concrete have resulted in high performance fiber-reinforced cementitious composites, which are characterized by tensile strain hardening after first cracking. Engineered cementitious composites (ECCs) invented by Li et al. [2,3] is micromechanically tailored by the addition of short fibers to achieve high ductility under tensile loading. Usually, ECC with a fiber content of at most 2% by volume strain-hardens after first cracking [4–6], and achieves a tensile strain capacity above 2%. The large deformation capacity is physically associated with formation of multiple fine cracks, and the crack width of ECC can be effectively controlled below 100 μm, even up to the final failure. In terms of permeability and diffusion, crack width less than 100 μm generally behaves like sound

concrete [7,8]. Therefore, by suppressing crack width even in presence of large imposed structural deformations, the use of ECC to replace normal concrete can effectively offer structural durability improvements, even completely eliminating steel reinforcement placed for the sole purpose of crack width control [7,9].

Unfortunately, broad applications of ECC material are hindered by its high cost, which can usually be reduced by employing a high volume of fly ash [10], substituting part of the oiled PVA fibers with unoiled PVA fibers [11], reducing the PVA fiber volume fraction from 2% to 1.5% [12], etc. Another effective method is to design ECC/reinforced concrete (ECC/RC) elements by replacing part of the concrete with ECC. To date, few research studies on mechanical behavior of ECC/RC composite members, especially bond behavior between ECC and concrete, have been conducted. Maalej and Li [13] first introduced ECC as a replacement for concrete material that surrounds the main reinforcement to improve durability of regular reinforced concrete structures. Leung and Cao [14] conducted an experimental study of composite beam with plain ECC formwork and discussed the effect of different formwork surface treatments on flexural behavior and durability of composite beam. Yuan et al. [15] evaluated the flexural behaviors of concrete/ECC composite beams reinforced with BFRP, and demonstrated that the strength and energy dissipation ability of composite beams are superior to the strength and energy dissipation ability of the concrete beam. Li and Xu [16] proposed a theoretical model to predict the flexural performance of functionally graded composite beams crack-controlled by ECC and then carried out an experiment to verify the validity of the proposed model.

In this paper, to help lower cost, we will first present the material design of cost-effective ECC with hybrid PVA fibers, and the determination of its mechanical properties. Then, U-shaped permanent formwork is made by this hybrid PVA-ECC, and the ECC/RC composite beam is further constructed by the casting of normal concrete. The bending test results on U-shaped ECC/RC composite beams with different formwork surface treatment are reported. Emphasis will be placed on flexural performance, especially bonding behavior between the formwork and the cast concrete, as well as the control of cracking by the ECC. This is followed by the development of theoretical model based on strip method to determine load-deflection response of composite beam. Finally, a simplified method is proposed to predict flexural capacity of U-shaped ECC/RC composite beam for convenience in practical design.

2 Optimal design of mix proportion of cost-effective PVA-ECC

2.1 General guideline

In the present research, the fiber used in ECC focuses on polyvinyl alcohol (PVA) fiber. Two types of PVA fibers, i.e., oiled and unoiled PVA fibers, are used in this study, and the dimensional information and mechanical properties are listed in Table 1. As shown in Table 1, unoiled PVA fibers and oiled PVA fibers are similar in tensile strength and elastic modulus. The price of unoiled fiber, however, is just approximately 1/8 of the price of the oiled fiber. Unoiled PVA fiber produced by Jiangsu Subote New Materials Co., Ltd., China, may be ruptured due to the strong chemical bonding to cement hydrates, and unoiled PVA-ECC can hardly exhibit good pseudo-strain-hardening performance [11]. Therefore, oiled fiber produced by Kuraray Co., Ltd., Japan is tailored by applying oil coating to the surface of the fiber to decrease the bond. In this case, it is worth studying the hybrid PVA-ECC to make it more feasible to apply ECC in large-scale practical engineering. The cost-effective ECC with hybrid PVA fibers at a dosage of 1% oiled fibers and 0.6% unoiled fibers in volume is engineered in this study, based on the feasibility analysis proposed by Pan et al. [11]. Since a significant part of the fly ash will act as inert filler leading to a loss of compressive strength [17], silica fume is added into the mixture in this study.

2.2 Mix proportion of cost-effective PVA-ECC

The mortar matrix of hybrid PVA-ECC consisted of Portland cement (P.II.42.5), silica sand (average size of 110 μm, and maximum size of 300 μm), first-grade fly ash, fumed silica, water, and polycarboxylic-type water reducer, as shown in Table 2. The manufacturing process will be described in detail as follows. Cement, silica sand, fumed silica, and fly ash were first mixed at low speed for approximately one and a half minutes. Water and water-reducing admixture were then added into the dry mixture and mixed for another three minutes. Once a consistent mixture was achieved, PVA fibers were slowly added into the mortar mixture until all fibers were uniformly distributed in the cement paste. The whole mixing procedure typically took approximately ten minutes.

2.3 Four-point bending test

Four specimens were cast with the same size of 350 mm ×

Table 1 Comparison of parameters of mechanical properties of PVA fiber

type	diameter (μm)	length (mm)	elongation (%)	density (g/cm^3)	elastic modulus (MPa)	nominal strength (MPa)
unoiled	26	12	7	1.3	36.3	1560
oiled	39	12	7	1.3	42.8	1620

50 mm × 15 mm (length × width × depth). The specimens were demolded after one day, then stored in a moist room. After 28 days, the specimens were removed from the curing room, and the age at testing was 300 days. Each specimen was loaded with four-point bending in a hydraulic servo-loading system. The loading span between two supports was 300 mm with a constant moment span length of 100 mm. A linear variable differential transformer (LVDT) was arranged at the center of the specimen to obtain the displacement at the midspan. The specimens were loaded by a displacement control with loading rate of 0.5 mm/min to achieve the softening behavior of the member.

The load versus midspan-deflection curves for specimens are shown in Fig. 1. At the beginning of loading, all specimens were in the elastic stage. With increasing applied loading, the first flexural crack generally occurs at the location with maximum flaw size in the constant moment region, accompanied by a decrease in the slope of curves relative to the initial linear behavior. As with oiled PVA-ECC [11], multiple fine cracks formed at the base of specimens, allowing them to undergo a strain-hardening stage with a large deflection. Finally, the dominant crack appears to propagate unsteadily and finally leads to the failure of the specimens. Compared with oiled PVA-ECC, the hybrid PVA fibers tend to decrease the ductility of ECC [11], but the ultimate midspan deflection of hybrid PVA-ECC is still observed up to 15.5 mm on average. The corresponding flexural strength of 10.9 MPa can be obtained in the test. Specially, the maximum crack width of specimens under the peak load is approximately only 160 μm.

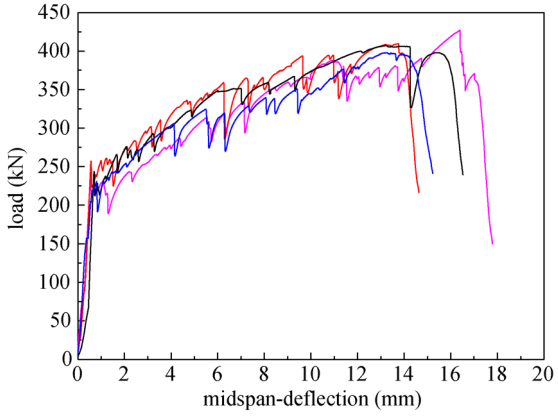

Fig. 1 Experimental load versus midspan-deflection curves of hybrid PVA- ECC.

2.4 Uniaxial compressive test

Three prism specimens (100 mm × 100 mm × 300 mm) were made for determining the compressive strength and elastic modulus. These specimens were cured in a standard manner for 28 days and then moved to air-dry until tested at the age of 300 days. All specimens were tested by a displacement control in a 3000 kN capacity hydraulic servo-loading system, and the loading rate was 0.3 mm/min.

The strength development curves of the specimens are shown in Fig. 2. As shown in Fig. 2, the compressive properties of ECC are significantly different from normal concrete. These specimens attain a compressive strength of approximately 43.5 MPa at a higher strain of 0.58%, with an elastic modulus of approximately 19.8 GPa, typically lower than concrete due to the lack of coarse aggregates. The post-peak behavior of ECC under compression tends to be gentler without obvious surface spalling instead of the sudden explosive crushing failure of concrete. Note that the type of PVA fibers has little effect on the compressive property of ECC [11], and thus the use of hybrid PVA fibers is feasible in terms of cost and compressive property.

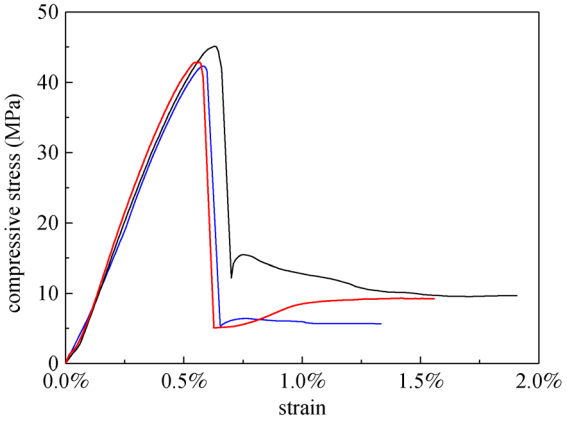

Fig. 2 Experimental compressive stress-strain curves of hybrid PVA-ECC.

3 Experimental program

3.1 Material properties

The reinforced specimens were provided with deformed steel rebar of 10 mm diameter with a yielding strength of 498 MPa for longitudinal reinforcement as well as 6 mm diameter with a yielding strength of 521 MPa for shear reinforcement. Both types of reinforcement have an elastic modulus of approximately 200 GPa. The cost-effective ECC with hybrid PVA fibers is adopted in the following test. Material properties in uniaxial compression were obtained directly from a compressive test conducted above, while the uniaxial tensile behavior can be predicted by a four-point bending test. Based on the simplified inverse method proposed by Qian [18], the first cracking strength and ultimate tensile strength of hybrid PVA-ECC

can be evaluated as 3 MPa at 0.015% strain and 4 MPa at approximately 1.67% strain, respectively. The formulation of concrete was based on cement, coarse aggregates, sand, water, mineral admixture, and polycarboxylic-type water reducer, as detailed in Table 2. The compressive strength of concrete was 52.5 MPa, and the elastic modulus was 41.5 GPa. Obviously, the compressive strength of the concrete used in this study is greater than the compressive strength of ECC used in the composite beam, which was initially chosen like the expected compressive strength of this version of ECC.

3.2 Fabrication of the U-shaped permanent formwork

In this study, the U-shaped permanent formwork was recommended to be divided into three plates to cast. The two side plates should first be prepared, where several L-shaped reinforcements were embedded at intervals of 20 cm to prevent debonding failure between the side and bottom plates. After 14 wet curing days, the bottom plate was further cast into the formwork made by the two existing side plates, as shown in Fig. 3. To study the bond behavior between the ECC formwork and concrete, different kinds of surface treatment were introduced on the surface of the bottom plate before initial setting of ECC, which include smooth as-finished surface (N), surface with transverse grooves (T) and surface with partially embedded sand particles (S), as shown in Fig. 3. For S surface condition, the coarse sands with average size of 2 cm were uniformly distributed on the surface of the bottom plate and further pressed slightly to assure that a part of every particle should be embedded into the plate, while the transverse grooves with width of 2 cm and depth of 2 mm were designed on the surface of the bottom plate for T surface condition. Finally, the members were constructed by casting of ordinary concrete when the bottom plate is wet cured for another 14 wet curing days.

3.3 Test specimens

Four different types, totalling eight beams, including four duplicates, were tested to investigate the flexural behavior and crack control capacity of the ECC/RC composite beam with three different surface treatments. All the six composite beams as well as two RC control beams have the same cross-sectional dimension (120 mm width × 150 mm depth) and arrangement of reinforcements, as shown in Fig. 4. The thickness of the bottom plate is 30 mm to provide a proper cover to the reinforcement inside, while the side plates have a smaller thickness of 20 mm resulting in a reduced weight and thereby a reduced cost. The specimens were longitudinally reinforced with two steel bars with a diameter of 10 mm, while the crowd transverse reinforcements with a diameter of 6 mm were arranged at 80 mm spacing between the support and loading point to provide enough shear resistance. For each beam specimen, two 6-mm steel reinforcements were also employed as compressive reinforcement to support the hanging of stirrups along the beam. All these reinforcements were placed into the concrete. The real longitudinal reinforcement ratio of the experimental specimens appears to increase from 0.87% to 1.5%, considering the four longitudinal reinforcements used in the L-shaped reinforcement fabric for the facility of positioning. Details of the

Table 2 Mixture proportions of concrete and ECC

material	cement	fly ash	fumed silica	slag	sand	coarse aggregates	water	fibre		water reducer
								unoiled	oiled	
concrete	1	0.1	–	0.3	2.8	4.2	0.6	–	–	0.0075
ECC	0.92	3.2	0.08	–	1.5	–	1.2	0.6%	1.0%	0.0028

Fig. 3 Fabrication of the ECC permanent formwork.

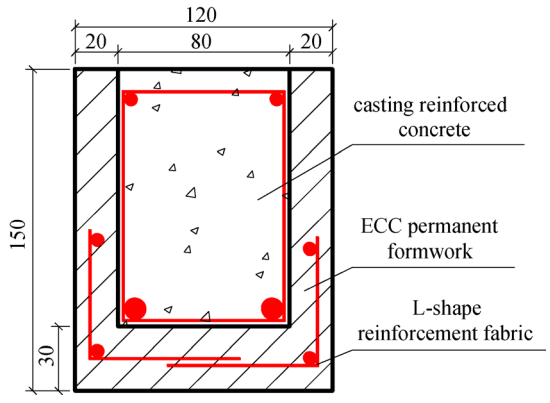

Fig. 4 Beam cross section details.

specimen configurations are summarized in Table 3. All beams were sealed in plastic bags cured in a 100%-humidity environment for 14 days as soon as the ordinary concrete was cast on the ECC formwork, and then left to air-dry until testing. The age at testing of the specimens was 300 days. Standard cuboid specimens (100 mm × 100 mm × 300 mm) for compression testing were also cast from the same matrix batch.

3.4 Test setup and test procedure

The schematic configuration of the test setup is shown in Fig. 5. Each beam was subjected to a four-point bending load with a span of 1200 mm between supports, which is applied symmetrically at 400 mm from the supports, resulting in a moderate shear span-depth ratio of 2.67 to avoid the shear failure. Three linear variable differential transformers (LVDTs) were used to monitor the midspan deflection of the beam, and two other LVDTs fixed on the top surface at the supports were employed to measure the support settlement under loading to correct the midspan deflection. To measure the yielding applied load, each longitudinal tensile bar as well as the L-shaped reinforcement fabric was instrumented with two strain gauges of 2 mm in length at constant moment span. A pair of strain gauges of 10 cm in length was attached to the top concrete and ECC surface of the beam, respectively, whose difference determines whether the debonding occurred between the two materials during the loading process. Seven strain gauges of 5 cm in length were fixed continuously at the bottom of the beam between two loading points to obtain the first cracking load. In the test, the vertical loading was applied with a 250 kN hydraulic actuator under displacement control at the rate of 0.5 mm/min and measured with a load cell. During the loading process, the data from strain gauges, LVDTs and the load cell are automatically collected by a data logger, and the crack width was measured by an instrument with a 150 mm × lens. For each specimen, the test was terminated when the applied load dropped to 50% of its peak load.

4 Experimental results and discussion

4.1 Models of failure

All the specimens with U-shaped ECC formworks showed the ductile flexural failure instead of the debonding failure before the crushing of the concrete, typically shown in Fig. 6. In terms of a higher longitudinal steel ratio leading to similarity between shear strength and flexural strength, one of the reference RC beams failed in combined flexural-shear after occurrence of diagonal crack localization, which implies that U-shaped ECC formwork can efficiently improve the shear strength of members by crack bridging force provided by PVA fibers. The strain difference between ECC and concrete on the top of the beam measured by strain gauges, as revealed in Fig. 7, appears to be approximately identical before the maximum load, which indicated the compatible deformation rather than delamination between ECC and concrete. With further increasing displacement, cracks caused by debonding were observed on the top of beam during the test, but the load does not drop suddenly due to debonding. Eventually, the composite beams all failed by the concrete crushing. In this case, the debonding is not the direct cause of member failure due to improvement in the interfacial resistance by increasing the interface area using U-shaped formwork even with smooth inner surface.

Table 3 Summary of specimen information

specimen	shear span-depth ratio	longitudinal reinforcement ratio (%)	shear reinforcement (mm)	matrix type	surface treatment
N-1	2.67	1.5	stirrups ϕ6@80	ECC/concrete	none
N-2	2.67	1.5	stirrups ϕ6@80	ECC/concrete	none
S-1	2.67	1.5	stirrups ϕ6@80	ECC/concrete	sand particles
S-2	2.67	1.5	stirrups ϕ6@80	ECC/concrete	sand particles
T-1	2.67	1.5	stirrups ϕ6@80	ECC/concrete	transverse grooves
T-2	2.67	1.5	stirrups ϕ6@80	ECC/concrete	transverse grooves
RC-1	2.67	1.5	stirrups ϕ6@80	ECC/concrete	–
RC-2	2.67	1.5	stirrups ϕ6@80	concrete	–

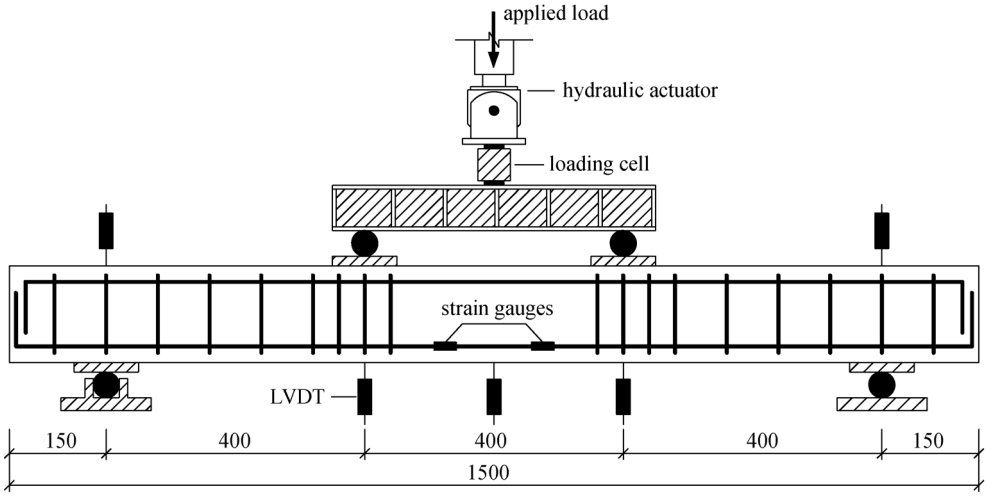

Fig. 5 Schematic of test setup.

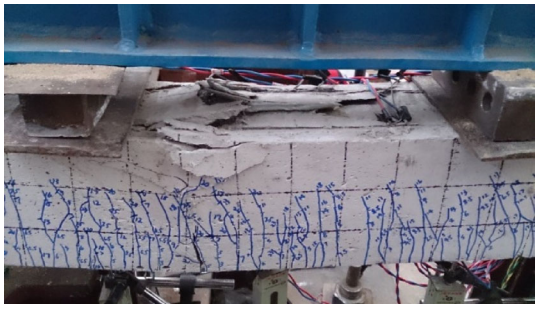

Fig. 6 Typical failure mode of the ECC/RC beam.

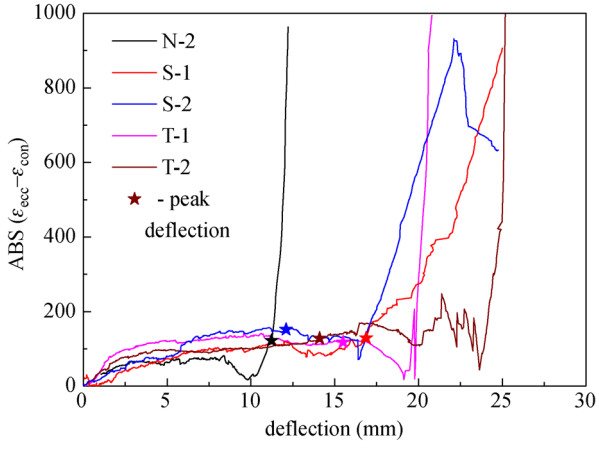

Fig. 7 Comparison of compressive strain of ECC and concrete at the top of the beams.

4.2 Load-deflection characteristics

The experimental load versus midspan-deflection curves of all specimens are given in Fig. 8. In this figure, a design load, which is calculated based on the strip method expatiated in the following section, is also shown. Figure 8 indicates that the load-deflection curves of ECC/RC specimens are similar to the curves of ordinary reinforced concrete specimens. All the composite beams exhibited the linear behavior until the first crack occurred. After the formation of cracks, the composite beams exhibited the nonlinear load-deflection characteristics and eventually failed in a ductile manner signified by the plateau in the load-deflection curve due to "yielding" of steel and ECC. Benefitting from the relatively ductile post-peak compressive behavior of ECC in the compressive zone, the failure process of composite beams was more gentle than RC beam. Unlike the flat plateau for RC beam, a softening behavior was observed in composite beams which indicated that the debonding between ECC and concrete has more effect on flexural behavior after peak load. Although debonding resulted in some undesirable loss in load, all composite beams failed by flexural crack localization rather than debonding crack localization.

The test results are summarized in Table 4. As shown in Table 4, the load-carrying capacity of ECC/RC composite beams all reached the design load, which demonstrated that interfacial debonding was not the dominant failure mode. The composite beams with a cracking load similar to the RC beam all achieved a larger yielding and ultimate load, approximately 14.0% and 14.1% higher than the concrete beams, as well as an improvement in deflection capacity denoted with ductility indices μ_{ult}/μ_{yield}. Generally, the composite beams showed a little increase in ductility compared with RC beams, since the ductility of the composite beam was also dominated by the ultimate compressive strain capacity of the concrete. A limited improvement in load-carrying capacity compared with the RC beam was also observed, since the contribution of ECC in the tension side to flexural capacity was relatively

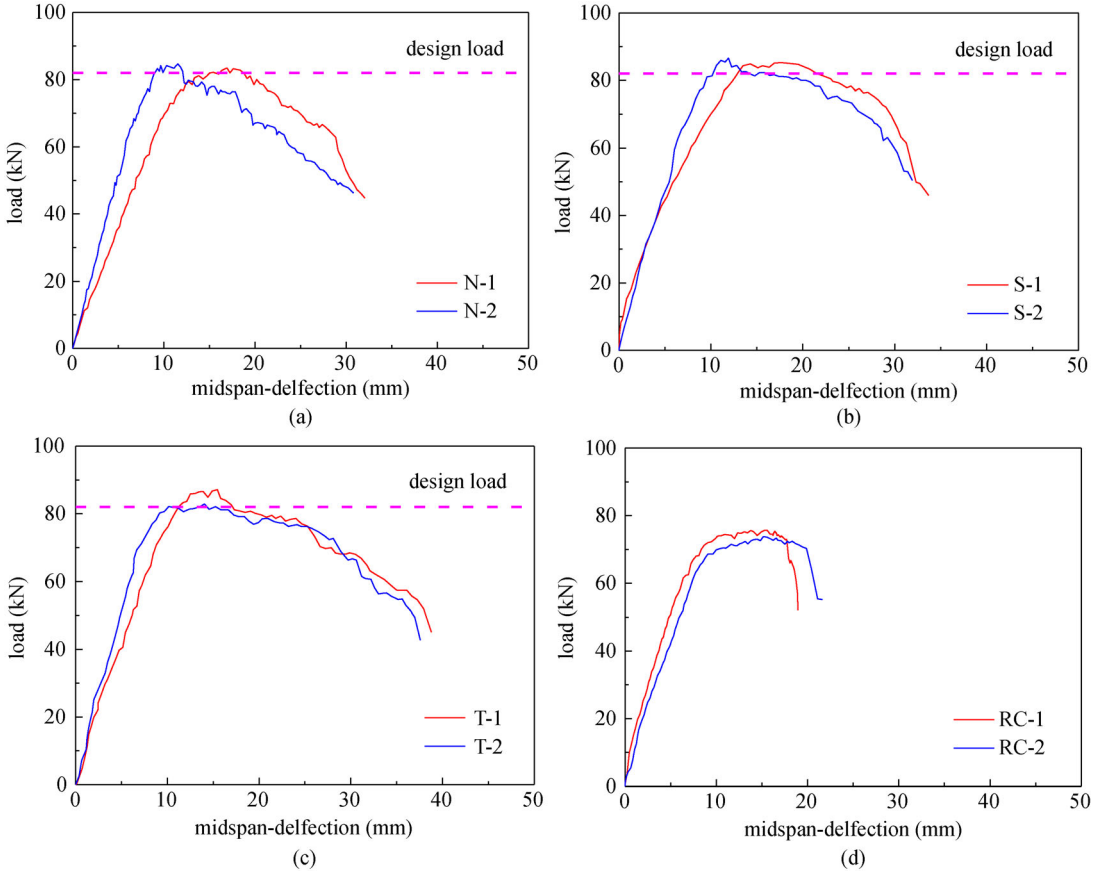

Fig. 8 Load versus midspan-displacement curve of all tested members. (a) Specimens N-1 and N-2; (b) specimens S-1 and S-2; (c) specimens T-1 and T-2; (d) specimens RC-1 and RC-2.

Table 4 Experimental results of tested beams

specimen	V_{cr} (kN)	μ_{cr} (mm)	V_{yeild} (kN)	μ_{yeild} (mm)	V_{peak} (kN)	V_{sim} (kN)	μ_{peak} (mm)	μ_{ult} (mm)	μ_{Δ} (mm)
N-1	9.5	0.58	65.5	9.1	83.6	78.9	16.8	26.5	2.91
N-2	10.4	0.43	70.1	7.2	84.6		11.5	19.7	2.74
S-1	9.8	0.28	72.8	9.7	85.3		16.2	28.1	2.89
S-2	9.3	0.46	68.8	7.5	87.1		12.1	25.7	3.43
T-1	11.1	0.56	70.8	8.4	87.2		15.5	28.2	3.36
T-2	8.4	0.51	73.1	7.1	82.9		14.0	30.6	4.31
strip method	10.2	0.34	74.5	6.5	82.5	–	22.4	22.4	3.45
RC-1	11.2	0.31	62.4	6.7	75.7	–	15.6	18.7	2.79
RC-2	9.9	0.39	58.4	7.1	73.8	–	15.2	20.8	2.93

Note: V_{cr} = the cracking load; μ_{cr} = midspan deflection at V_{cr}; V_{yield} = the yielding load when the main steel bar with 10 mm diameter yields; μ_{yeild} = midspan deflection at V_{yield}; V_{peak} = the peak load; μ_{peak} = midspan deflection at V_{peak}; μ_{ult} = the ultimate midspan deflection when the applied load decreases to 80% of the peak load; μ_{Δ}= ductility calculated by μ_{ult}/μ_{yield}.

degraded when the longitudinal steel ratio is relatively high. Another reason that can also explain this behavior is that the compressive strength of concrete used in this test is greater than the compressive strength of the ECC in the composite beam. The surface condition in the ECC/RC beams had little influence on the peak load, but it affected the ductility of the members. The surface with transverse grooves showed the best ductility because of the best interfacial bonding, followed by the surface with the embedded sand particles and the smooth as-finished surface. This is because that good interfacial bonding can enable the shear stress to be effectively transferred back to

the uncracked concrete, and thus more cracks in concrete occur accompanied by the formation of additional fine cracks in the ECC near these new concrete cracks. As a result, the ductility will be further improved.

4.3 Crack propagation and width

For RC beams, the first crack appeared randomly at the weak location in the pure bending zone. As the load increased, the flexural cracks propagated both in number and width. Beyond yielding, there are no new cracks formed in the concrete, while the width of existing cracks increases dramatically up to failure. For ECC/RC composite beams, the cracks formed in concrete will be arrested by the formwork and then diffused into numerous fine cracks in the ECC layer due to the crack bridging force provided by the PVA fibers. Note that the number of cracks in the ECC increased continuously up to the localization of the major crack, and crack width, in the meanwhile, remained almost constant, usually less than 200 μm. Figure 9 depicts the crack pattern in all specimens observed after failure. As expected, there are large numbers of fine cracks at the constant moment region of the composite beam rather than several wide cracks in the

Fig. 9 Crack pattern in tested beams after ultimate failure. (a) Specimen N-1; (b) specimen N-2; (c) specimen S-1; (d) specimen S-2; (e) specimen T-1; (f) specimen T-2; (g) specimen RC-1; (h) specimen RC-2.

RC beams. Therefore, it is fair to assert that the serviceability limit controlled by crack width will no longer govern the design of flexural members for the ECC/RC composite beam, since the small crack width of the ECC matrix should enhance durability of structures.

The maximum crack width measured at constant moment span verses normalized load capacity for all tested specimens are revealed in Fig. 10. Normalized load capacity in this figure is the ratio of applied load to the peak load. Figure 10 shows that the crack width of the RC beam tends to increase dramatically even up to 1 mm after the yielding of the steel, while increase of the crack width of ECC/RC composite beam can stabilize less than 400 μm before the peak load. It is remarkable that the crack width does not even exceed 100 μm when the applied load is less than 80% of the peak load. As specified by AASHTO [19] for outdoor exposures, a crack width of 0.3 mm was used to represent the serviceability limit of reinforced concrete structures, and the corresponding service load is usually approximately 50% to 70% of the design load [20]. Crack width control is of primary importance for many reinforced concrete applications, since it is believed that there is a close relationship between maximum crack width and the durability of the structure. As pointed out by research studies [8,21], the formation of the crack is perceived to have a limited effect on the transport property of the matrix when its width is below 100 μm. Therefore, there is substantial potential for ECC to transfer its material ductility to durability of the structure by acting as a quality cover such as the U-shaped formwork even exposed in a severe environment.

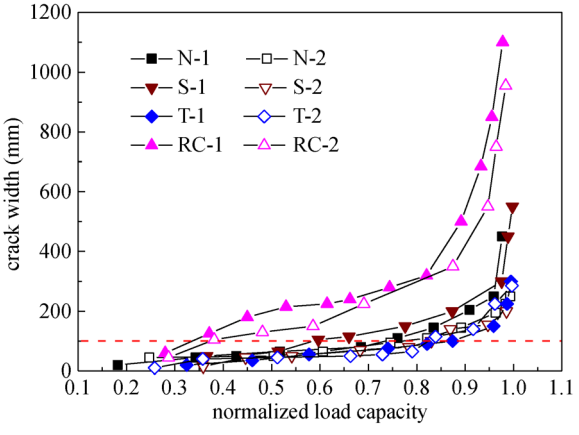

Fig. 10 Crack width versus normalized applied load curve.

As a material specially tailored by a micromechanical model, the ECC with tension strain capacity beyond 3% can be obtained easily [2,3], and yet the resulting cost will increase dramatically. Hence, ECC should be tailored to accommodate performance demands for different applications. For the structures emphasizing lower damage tolerance under extreme loading such as earthquake and typhoon, the ECC with tensile strain capacity in excess of 3%, which can ensure that no strain localization will take place in the ECC formwork, is preferable to replace part of the concrete in key components. For the structures exposed to an aggressive environment, it is effective in meeting the requirement of durability to introduce the ECC to serve as a quality cover with moderate tensile strain capacity less than 1.5%, since the service load is only 50%–70% of the design load.

4.4 Analytical load-deflection relationship

The strip method is adopted in this study to calculate the load-deflection relationship of the tested beams, and several assumptions are made for simplicity:

1) Cross section remains level during the whole deformation process.

2) There is no interface slip between concrete and ECC during calculation.

3) In this study, the stress-strain relationship of ECC in tension is simplified by a bilinear curve [22], as shown in Fig. 11(a). The expression for tensile stress-strain relationship is given as follows:

$$\sigma_{et}=\begin{cases}\dfrac{f_{etc}}{\varepsilon_{etc}}\varepsilon_t, & 0\leqslant\varepsilon_t\leqslant\varepsilon_{etc},\\ f_{etc}+\dfrac{f_{etu}-f_{etc}}{\varepsilon_{etu}-\varepsilon_{etc}}(\varepsilon_t-\varepsilon_{etc}), & \varepsilon_{etc}\leqslant\varepsilon_t\leqslant\varepsilon_{etu},\end{cases}\tag{1}$$

where f_{etc} and f_{etu} are the first cracking tensile strength and the ultimate tensile strength, respectively; ε_{etc} and ε_{etu} are the strain corresponding to f_{etc} and f_{etu}, respectively.

4) The widely used uniaxial compressive model for concrete proposed by Hognestad et al. [23] is adopted with a slight modification for ECC material, as shown in Fig. 11(b). Based on the compressive test results in this study, a shape factor ζ of ECC is suggested to be 1.35 instead of the constant value of 2 for normal concrete due to the relatively lower elastic modulus of ECC. The expression of the compressive stress-strain curve is given as follows:

$$\sigma_{ec}=\begin{cases}f_{ec}\left[\zeta\dfrac{\varepsilon_c}{\varepsilon_{e0}}+(1-\zeta)\left(\dfrac{\varepsilon_c}{\varepsilon_{e0}}\right)^2\right], & \varepsilon_c\leqslant\varepsilon_{e0},\\ f_{ec}+(f_{ecu}-f_{ec})\left(\dfrac{\varepsilon_c-\varepsilon_{e0}}{\varepsilon_{ecu}-\varepsilon_{e0}}\right), & \varepsilon_{e0}<\varepsilon_c\leqslant\varepsilon_{ecu},\\ f_{ecu}, & \varepsilon_{ecu}<\varepsilon_c,\end{cases}\tag{2}$$

where ε_{e0} is the compressive strain at peak stress f_{ec}; f_{ecu} is the residual stress, and ε_{ecu} is the strain corresponding to f_{ecu}, which is usually equal to $1.2\varepsilon_0$.

5) As shown in Fig. 12, an elastic tensile stress-strain relationship is used before cracking for concrete, while the compression constitutive model of concrete proposed by

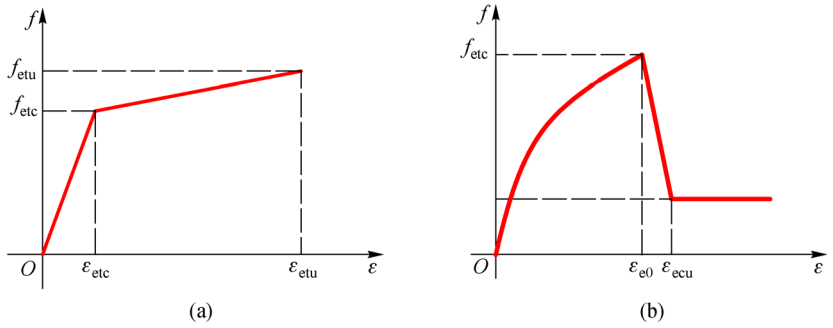

Fig. 11 Stress-strain relationship of ECC. (a) Under uniaxial tension; (b) under uniaxial compression.

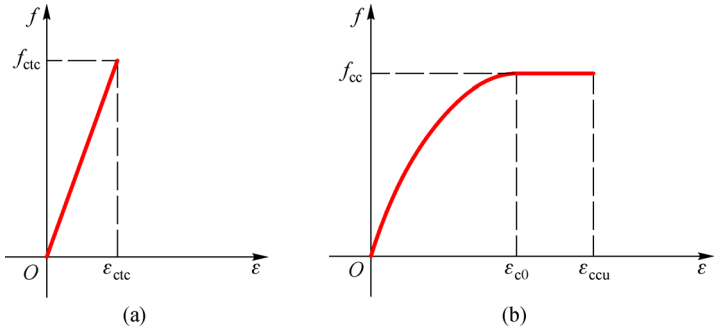

Fig. 12 The stress-strain relationship of concrete. (a) Under uniaxial tension; (b) under uniaxial compression.

Rüsch [24] is adopted for simplicity. The expression of the tensile and compressive stress-strain curve is given as follows:

$$\sigma_{ct}=\begin{cases}\dfrac{f_{ctc}}{\varepsilon_{ctc}}\varepsilon_t, & 0\leqslant\varepsilon_t\leqslant\varepsilon_{ctc},\\ 0, & \varepsilon_{ctc}<\varepsilon_t,\end{cases} \tag{3}$$

$$\sigma_{cc}=\begin{cases}f_{cc}\left[\dfrac{2\varepsilon_c}{\varepsilon_{c0}}-\left(\dfrac{\varepsilon_c}{\varepsilon_{c0}}\right)^2\right], & 0\leqslant\varepsilon_c\leqslant\varepsilon_{c0},\\ f_{cc}, & \varepsilon_{c0}<\varepsilon_c\leqslant\varepsilon_{ccu},\end{cases} \tag{4}$$

where ε_{ctc} and f_t are the cracking strain and tensile strength, respectively; ε_{c0} is the compressive strain at the peak stress f_{mL}; ε_{ccu} is the ultimate compressive strain.

6) To simplify the analysis, the perfect elastic-plastic model of steel bar can be expressed by the following formulas:

$$\sigma_s=\begin{cases}E_s\varepsilon_s, & 0\leqslant\varepsilon_s\leqslant\varepsilon_y,\\ f_y, & \varepsilon_y\leqslant\varepsilon_s,\end{cases} \tag{5}$$

where E_s is the elastic modulus; ε_y and f_y are the yielding strain and yielding stress, respectively.

In strip method [25], the cross section is first discretized into numerous strips. To start the procedure, a tensile strain at extreme tensile fiber ε_t is assigned. The distance of neutral axis c from the bottom is calculated from force equilibrium of the section based on the assumed stress-strain relationships, and the corresponding moment is obtained by summing the moment contributions from individual layers about the neutral axis. For a constant curvature [22], the maximum deflection f for a beam having a span of L is given by

$$f=\frac{L^2\varepsilon_t}{8c}. \tag{6}$$

Repeating the calculation with different values of ε_t, the load-deflection relationship of a ECC/RC composite beam can be determined. Particularly, the ultimate state of the beam is assumed to be reached when the strain at extreme compression fiber ε_c reaches the ultimate compressive strain of concrete ε_{ccu}.

The comparison of load-deflection response between the experimental and calculated results is shown in Fig. 13. The load-carrying capacities, including cracking load V_{cr}, yielding load V_{yeild}, and ultimate load V_{peak}, and corresponding deflections were picked up from the calculated curve and are shown in Table 4. As revealed in Fig. 13 and Table 4, the theoretical load-deflection curve shows a good agreement with the tested results, especially the load-carrying capacities can be predicted satisfactorily. It is true that the difference of deflection between the experimental results and the calculated result is small before reinforcement yields but slightly large beyond yielding, mainly due to no consideration of interfacial debonding between ECC and concrete. The Eq. (6) is derived based on mechanics of materials under large deformation where a constant curvature along the long-

itudinal direction of specimens is assumed [22], and thus the initial elastic modulus of the calculated curve is higher than experimental results.

Another issue related to the flexural behavior of the reinforced ECC beam and U-shaped ECC/RC composite beam is evaluated through two examples calculated by the strip method. The geometric and mechanical parameters of two examples are all the same as the parameters of experimental beams. To assess the flexural behavior of two examples objectively, the compressive strength of concrete had better be identical with the compressive strength of ECC (43.5 MPa). Figure 14 presents the predicted load-deflection curve of these two examples. As shown in Fig. 14, the reinforced ECC beam shows a 7.2% higher load at the ultimate state than the load of the composite beam, and a remarkable improvement of 20% in deflection capacity is also observed because the failure of the RECC beam is dominated by the ultimate compressive strain of ECC, which is higher than the ultimate compressive strain of concrete. In practice, considering the rational interface slip of concrete and ECC, the deflection capacity of the composite beam may be close to the deflection capacity of the RECC beam without a sudden load drop. Therefore, we can conclude that there is no need to replace all the concrete with ECC in terms of flexural performance and cost.

5 Simplified solution of flexural capacity

In this study, the simplified solution of flexural capacity is derived not only for ECC but also for other synthetic short fiber-reinforced cement composites that exhibit pseudo-strain-hardening behavior and multiple fine cracking behavior under uniaxial tensile stress conditions.

5.1 Fundamental assumption

The assumption adopted in simplified analysis is identified with that used in the strip method, except that the tensile and compressive constitutive models of ECC are further simplified as shown in Fig. 15. Specifically, the strain-hardening behavior of ECC after cracking is neglected, and then the Eq. (1) can be simplified to

$$\sigma_{et}=\begin{cases}\dfrac{f_{etc}}{\varepsilon_{etc}}\varepsilon_t, & 0\leqslant\varepsilon_t\leqslant\varepsilon_{etc},\\ f_{etc}, & \varepsilon_{etc}\leqslant\varepsilon_t\leqslant\varepsilon_{etu}.\end{cases}\tag{7}$$

Like normal concrete, the simplified compressive constitutive model of ECC can be expressed by the following formulas:

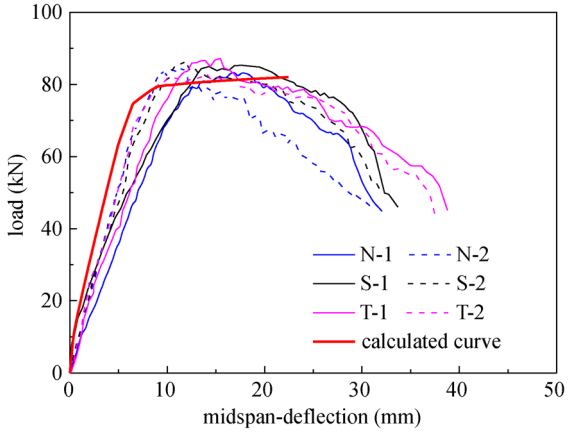

Fig. 13 Comparison between calculated and experimental load-deflection responses.

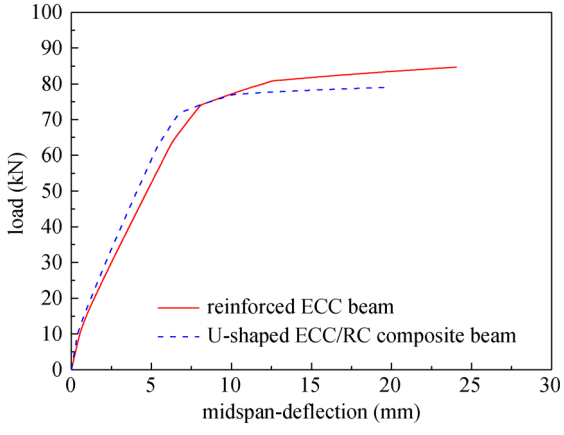

Fig. 14 The calculated load-deflection relationship of the examples.

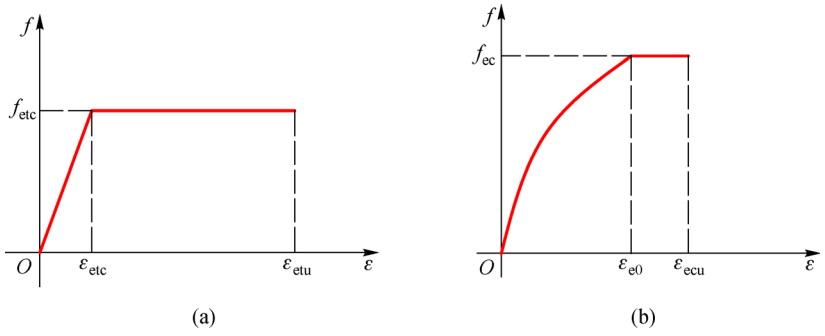

Fig. 15 Simplified stress-strain relationship of ECC. (a) Under uniaxial tension; (b) under uniaxial compression.

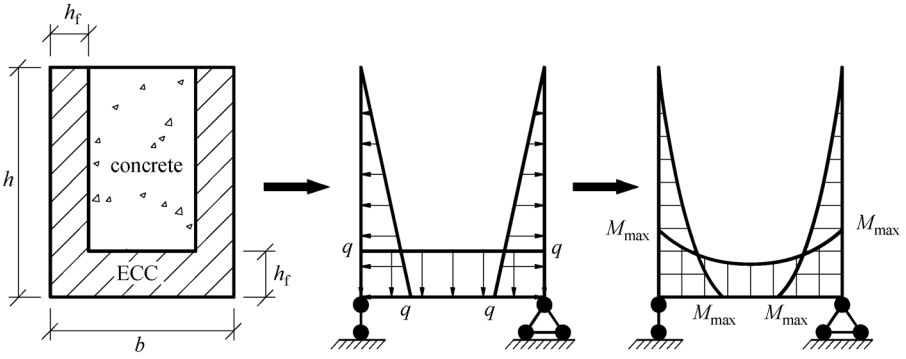

Fig. 16 Simplified model and moment distribution of U-shaped ECC formwork.

$$\sigma_{ec}=\begin{cases} f_{ec}\left[\zeta\dfrac{\varepsilon_c}{\varepsilon_{e0}}+(1-\zeta)\left(\dfrac{\varepsilon_c}{\varepsilon_{e0}}\right)^2\right], & \varepsilon_c\leqslant\varepsilon_{e0},\\ f_{ec}, & \varepsilon_{e0}<\varepsilon_c\leqslant\varepsilon_{ecu}. \end{cases} \tag{8}$$

5.2 The optimal thickness of U-shaped ECC formwork

Based on the foregoing analysis, U-shaped ECC permanent formwork is employed mainly as a protective layer to improve the durability of RC structure. Therefore, the thicknesses of the side and bottom plates in the ECC formwork are expected to exceed the specified cover for reinforcement h_c such as 50.8 mm for the beam exposed to weather provided by ACI 318-14 [26]. With a reduced thickness, transportation and handling is facilitated by a reduced weight, and the formwork cost is also reduced.

Another issue related to thickness of formwork is that when the normal concrete is cast into an ECC formwork, the two materials cannot work as a whole and thereby additional distributed load will be applied to the ECC formwork by fresh concrete, which tends to put the formwork at the risk of cracking. The simplified mechanical model and corresponding moment distribution of the U-shaped ECC formwork are shown in Fig. 16. As shown in Fig. 16, the U-shaped ECC formwork is simplified to a simply supported system under lateral and vertical distributed load applied by fresh concrete during casting. The maximum moment M_{max} is reached at the junction of side plate and bottom plate, and its value is determined only by the depth of section h. Herein, the maximum moment M_{max} is given by

$$M_{max}=\frac{qh^2}{6}, \tag{9}$$

$$q=\rho_c g h b_l, \tag{10}$$

where q is the maximum value of distributed load; ρ_c is the density of concrete and is usually deemed to be 2400 kg/m^3 for normal concrete; g is the acceleration of gravity and is equal to approximately 10 N/kg; and b_l is longitudinal calculating length of formwork and can be taken as unit length for convenience.

To avoid cracking of U-shaped ECC formwork during casting of concrete, the maximum moment of plate M_{max} cannot exceed its cracking moment M_{cr}. As specified in ACI 318-14, cracking moment M_{cr} for a rectangular section can be obtained by

$$M_{cr}=\frac{f_r b_l h_f^2}{6}, \tag{11}$$

where h_f is the thickness of the side plate or the bottom plate; f_r is the modulus of cracking of ECC, which can be derived inversely from Eq. (11) based on the cracking moment measured by the four-point bending test or the three-point bending test. Then, the minimum thickness of plates of ECC formwork h_{min} can be calculated by

$$h_{min}=\sqrt{\frac{\rho_c g H^3}{f_r}}. \tag{12}$$

Thus, considering both durability and economy of the composite beam, the optimal thickness of the U-shaped ECC formwork h_p can be determined by

$$h_p\geqslant\max\{h_c,h_{min}\}. \tag{13}$$

Particularly, if the optimal thickness h_p exceeds $2h_c$, it is certainly preferable to put several longitudinal tensile reinforcements located in concrete into the ECC formwork.

5.3 Flexural capacity

For U-shaped ECC/RC composite beam, when the strain at extreme compression fiber ε_c reaches the ultimate compressive strain of concrete ε_{ccu}, the failure of the composite beam occurs with a section moment M_u, which is defined as the flexural capacity of the composite beam at the ultimate stage. In this case, the stress and strain distribution in either compression region or tension region is shown in Fig. 17. For simplicity, the ECC material in the

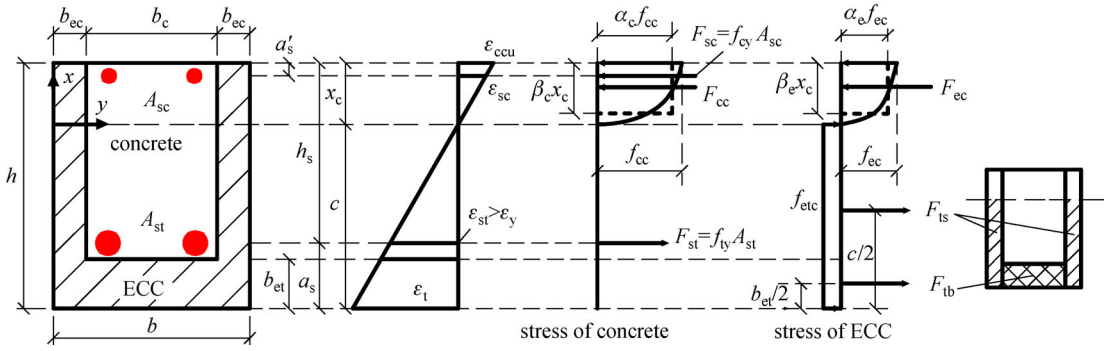

Fig. 17 The distribution of stress and strain along the depth of the composite beam.

tension region is all assumed to "yield" without regard to the elastic stage. As shown in Fig. 17, according to force equilibrium conditions, Eq. (14) can be obtained by

$$F_{cc} + F_{ec} + f_{cy}A_{sc} = F_{ts} + F_{tb} + f_{ty}A_{st}, \tag{14}$$

where F_{cc} and F_{ec} are the compression force of the concrete and the ECC, respectively; A_{sc} and f_{cy} are the area and yielding stress of compressive reinforcement, respectively; A_{st} and f_{ty} are the area and yielding stress of tensile reinforcement, respectively; and F_{ts} and F_{tb} are the tensile force of ECC in side plates and bottom plate of the formwork, respectively, which can be further expressed as

$$F_{ts} = 2b_{ec}f_{etc}(h - x_c), \tag{15}$$

$$F_{tb} = b_c b_{et} f_{etc}, \tag{16}$$

where b_{ec} and b_{et} are the thickness of the side plate and bottom plate in the ECC formwork, respectively; b_c is the width of the normal concrete; and x_c is the depth of the compression zone. Integration of the compressive stress blocks of concrete and ECC gives

$$F_{cc} = b_c \int_0^{x_c} \sigma_{cc}\left(\frac{x\varepsilon_{ccu}}{x_c}\right)\mathrm{d}x, \tag{17}$$

$$F_{ec} = 2b_{ec} \int_0^{x_c} \sigma_{ec}\left(\frac{x\varepsilon_{ccu}}{x_c}\right)\mathrm{d}x, \tag{18}$$

where $\sigma_{cc}(\varepsilon)$ and $\sigma_{ec}(\varepsilon)$ give the simplified compressive stress-strain relationship of concrete and ECC, respectively; x is the distance from a compression fiber to the neutral axis (Fig. 17).

For the convenience of practical engineering design, the stress of concrete in the compression side can be simplified to an equivalent rectangle as shown in Fig. 17, when the strain at the extreme compression fiber reaches the ultimate limit state. The α_c is the ratio of average compressive stress to f_{mL} which is equal to 0.85 for normal concrete as in ACI 318-14 [26], while the β_c is the ratio of depth of equivalent rectangular stress-block to depth of neutral axis which varies from 0.65 to 0.85 as

$$\beta_c = \begin{cases} 0.85, & f_{cc} \leqslant 28\ \text{MPa}, \\ 0.85 - 0.05(f_{cc} - 28)/7, & 28\ \text{MPa} < f_{cc} \leqslant 55\ \text{MPa}, \\ 0.65, & f_{cc} > 55\ \text{MPa}, \end{cases} \tag{19}$$

which leads to

$$F_{cc} = \alpha_c f_{cc} b_c \beta_c x_c. \tag{20}$$

Similarly, the equivalent rectangular stress distribution approach is also adopted for the stress of ECC on the compressive side, and the compressive force of ECC F_{ec} can be given by

$$F_{ec} = 2\alpha_e f_{ec} b_{ec} \beta_e x_c, \tag{21}$$

where α_e and β_e for ECC have the same meaning as α_c and β_c for concrete, respectively. α_e and β_e can be obtained based on the compressive stress-strain relationship of ECC as well as two equivalent principles, i.e., compression force and the centroid of compression force remain unchangeable for the equivalent rectangular and actual stress distribution. The compressive strain of concrete at which ultimate moments are developed is usually approximately 0.3% to 0.4% for members of normal concrete, while the compressive strain capacity of ECC is slightly higher, approximately 0.45%–0.65%, which implies that ECC on the compressive side has not reached its ultimate limited state when the ECC/RC composite beam failed by concrete crushing. Therefore, it is necessary to evaluate α_e and β_e at a certain given strain ε_c in an extremely compressive region and the corresponding mathematical expressions can be written as follows:

for $\varepsilon_c \leqslant \varepsilon_{e0}$,

$$\alpha_e = \left\{\frac{\zeta\,\varepsilon_c}{2\,\varepsilon_{e0}} + \frac{1-\zeta}{3}\left(\frac{\varepsilon_c}{\varepsilon_{e0}}\right)^2\right\}/\beta_e, \tag{22}$$

$$\beta_e = 2 - \frac{\dfrac{2\zeta}{3} + \dfrac{1-\zeta\,\varepsilon_c}{2\ \ \varepsilon_{e0}}}{\dfrac{\zeta}{2} + \dfrac{1-\zeta\,\varepsilon_c}{3\ \ \varepsilon_{e0}}}, \tag{23}$$

for $\varepsilon_{e0} < \varepsilon_c \leqslant \varepsilon_{ecu}$,

$$\alpha_e = \left[1 + \left[\frac{\zeta}{2} + \frac{1-\zeta}{3} - 1\right]\frac{\varepsilon_{e0}}{\varepsilon_c}\right]/\beta_e, \tag{24}$$

$$\beta_e = 2 - \frac{1 + \left[\frac{2\zeta}{3} + \frac{1-\zeta}{2} - 1\right]\left(\frac{\varepsilon_{e0}}{\varepsilon_c}\right)^2}{1 + \left[\frac{\zeta}{2} + \frac{1-\zeta}{3} - 1\right]\frac{\varepsilon_{e0}}{\varepsilon_c}}. \tag{25}$$

Obviously, α_e and β_e are found dependent on ζ and ε_{e0}. For the hybrid PVA-ECC in this study, the shape factor ζ of 1.35 is introduced based on the compressive test results. Therefore, the influence of different ε_{e0} on the α_e and β_e at the given ε_c is investigated, and the results are presented in Table 5. Table 5 shows that when ε_c is equal to ε_{e0} or ε_{ecu} (equal to $1.2\varepsilon_{e0}$ for hybrid ECC), the value of α_e and β_e are certainly independent of ε_{e0} and remain constant at 0.70 and 0.80 for $\varepsilon_c = \varepsilon_{e0}$ and 0.72 and 0.88 for $\varepsilon_c = \varepsilon_{ecu}$, respectively. Moreover, the value of ε_{e0} has little effect on β_e at different ε_c, and thereby β_e is averaged to be 0.685 for $\varepsilon_c \leqslant \varepsilon_{e0}$ and 0.70 for $\varepsilon_c > \varepsilon_{e0}$, respectively. Then, upon the introduction of β_e into Eqs. (22) and (24), α_e can be attained.

Based on the foregoing analysis, replacing Eqs. (15) – (25) into Eq. (14) gives

$$\begin{aligned}&\alpha_c f_{cc} b_c \beta_c x_c + 2\alpha_e f_{ec} b_{ec} \beta_e x_c + f_{cy} A_{sc} \\ &\quad = b_c b_{et} f_{etc} + 2 b_{ec} f_{etc}(h - x_c) + f_{ty} A_{st}.\end{aligned} \tag{26}$$

The depth of the compression zone x_c can be calculated by Eq. (26) when $\varepsilon_c = \varepsilon_{ccu}$ and corresponding ultimate moment of ECC/RC section M_u can be further obtained by

$$\begin{aligned}M_u &= F_{cc}\left(h_s - \frac{\beta_c x_c}{2}\right) + F_{ec}\left(h_s - \frac{\beta_e x_c}{2}\right) \\ &\quad + f_{cy} A_{sc}\left(h_s - a_s'\right) - F_{ts}\left(\frac{h - x_c}{2} - a_s\right) \\ &= \alpha_c f_{cc} b_c \beta_c x_c \left(h_s - \frac{\beta_c x_c}{2}\right) \\ &\quad + 2\alpha_e f_{ec} b_{ec} \beta_e x_c \left(h_s - \frac{\beta_e x_c}{2}\right) \\ &\quad + f_{cy} A_{sc}\left(h_s - a_s'\right) - 2 b_{ec} f_{etc}(h - x_c)\left(\frac{h - x_c}{2} - a_s\right),\end{aligned} \tag{27}$$

where a_s is the distance between the centroid of tensile reinforcement and extreme tension fiber; a_s' is the distance between the centroid of compressive reinforcement and extreme compression fiber; and h_s is the effective depth calculated by $h - a_s$. As the centroid of F_{tb} is close to the centroid of tensile reinforcement, especially when tensile reinforcements were arranged in bottom plate of ECC formwork, the contribution of F_{tb} to the section moment is neglected conservatively in Eq. (27). The derivation of Eq. (27) is based on two assumptions. The first assumption is that all reinforcements yield before the onset of flexural capacity M_u. The strain of compressive reinforcement ε_{cs} shall exceed its yielding strain ε_{cy}, i.e., $\varepsilon_{cs} \geqslant \varepsilon_{cy}$. Based on Fig. 17, one has

$$\frac{\varepsilon_{cs}}{\varepsilon_{ccu}} = \frac{x_c - a_s'}{x_c}, \tag{28}$$

which leads to

$$x_c \geqslant \frac{1}{1 - \frac{\varepsilon_{cy}}{\varepsilon_{ccu}}} a_s' = \frac{1}{1 - \frac{f_{cy}}{E_{cs}\varepsilon_{ccu}}} a_s'. \tag{29}$$

The other assumption is that the strain of ECC on the tensile side remains below its ultimate tensile strain ε_{etu} during the whole bending process. For the structures not in a seismic zone but exposed to an aggressive environment, an advisable ultimate tensile strain capacity of ECC used in formwork, which can ensure requirement of durability at serviceability limit state in terms of crack width, was preferable. In this case, the strain of partial ECC on the tensile side of the composite beam may exceed its ultimate tensile strain accompanied by a reduced flexural capacity M_{ur} at the ultimate limit state. According to the coordinate transformation in Fig. 17, the strain of ECC at extreme tensile fiber ε_t can be expressed by

$$\varepsilon_t = \frac{(h - x_c)\varepsilon_{ccu}}{x_c}. \tag{30}$$

Substituting the solution of x_c in Eq. (26) into Eq. (30) gives ε_t at the ultimate limit state. If ε_t exceeds the tensile stain capacity of ECC ε_{etu}, Eq. (27) is unavailable due to invalidation of the assumption, and x_c should be recalculated. On this occasion, the real depth of ECC x_t sustaining tensile force is given by

Table 5 The value of α_e and β_e at different ε_c

ε_c	ε_{e0}									
	0.0045		0.005		0.0055		0.006		0.0065	
	α_e	β_e	α_e	β_e	α_e	β_e	α_e	β_e	α_e	β_e
0.001	0.21	0.67	0.19	0.67	0.18	0.67	0.16	0.67	0.15	0.67
0.003	0.58	0.69	0.53	0.69	0.49	0.68	0.45	0.68	0.42	0.68
ε_{e0}	0.8	0.7	0.8	0.7	0.8	0.7	0.8	0.7	0.8	0.7
ε_{ecu}	0.88	0.72	0.88	0.72	0.88	0.72	0.88	0.72	0.88	0.72

$$x_t = \frac{x_c \varepsilon_{etu}}{\varepsilon_{ccu}}, \tag{31}$$

which leads to

$$\alpha_c f_{cc} b_c \beta_c x_c + 2\alpha_e f_{ec} b_{ec} \beta_e x_c + f_{cy} A_{sc} = 2 b_{ec} f_{etc} x_t + f_{ty} A_{st}. \tag{32}$$

Since the value of F_{tb} here is relatively small and may even be equal to zero, its contribution to tension force is neglected in Eq. (32). The corresponding ultimate moment M_{ur} of ECC/RC section can be further expressed by

$$M_{ur} = \alpha_c f_{cc} b_c \beta_c x_c \left(h_s - \frac{\beta_c x_c}{2}\right) + 2\alpha_e f_{ec} b_{ec} \beta_e x_c \left(h_s - \frac{\beta_e x_c}{2}\right) + f_{cy} A_{sc} \left(h_s - a_s'\right) - 2 b_{ec} f_{etc} x_t \left(h - x_c - \frac{x_t}{2} - a_s\right). \tag{33}$$

5.4 Verification of simplified solution of flexural capacity

The simplified solution of flexural capacity is shown in Table 4 for specimens tested in this study. V_{sim} is the equivalent load-carrying capacity and equal to the value of calculated moment M_u or M_{ur} divided by the distance between support and loading point. The calculated results show that the simplified solution of flexural capacity has a rational agreement with the measured as well as the calculated by the strip method. To further verify the validity of the proposed simplified method, several numerical examples were selected for the simplified method and compared with the results calculated by the strip method. In these examples, four typical sectional dimensions of composite beam, i.e., 400 mm×200 mm, 600 mm×300 mm, 800 mm×400 mm, 1000 mm×500 mm, were investigated, and the corresponding thickness of formwork was designed by Eq. (13). The tensile reinforcement ratio and ultimate tensile strain capacity ε_{etu} of ECC both vary from 0.5% to 3%, while the compressive strength of concrete ranges from 30 to 60 MPa, and the other material parameters and geometric dimensions were identical with the tested specimens in this study. Figure 18 showed the comparison between the predicted flexural strength calculated by the simplified method and the strip method, denoted by M_{sim} and M_{str}, respectively. The data are almost distributed along the diagonal in the figure, in which the ratio of M_{sim} to M_{str} presents the mean of 1.01 and the CV of 0.02 of all examples. The good agreement between M_{sim} and M_{str} indicates that the simplified method can be used to predict flexural capacity of the U-shaped ECC/RC composite beam, whether the ultimate tensile strain capacity of ECC is enough or not to ensure that no crack localization takes place up to failure of the composite beam.

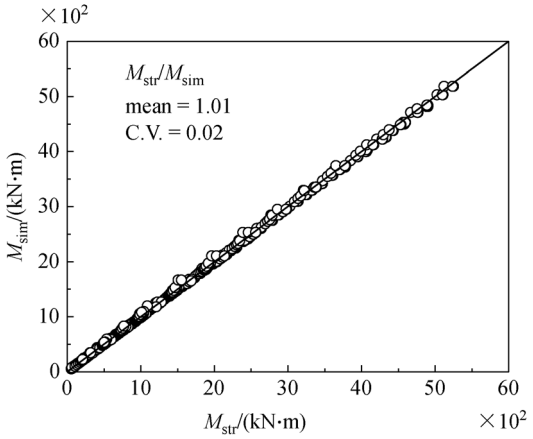

Fig. 18 Comparison between the predicted flexural strengths calculated by simplified method (M_{sim}) and strip method (M_{str}).

6 Conclusions

To reduce the production cost of ECC, the hybrid PVA-ECC is first proposed, and then its mechanical properties are studied experimentally. Furthermore, experimental and theoretical investigation of the flexural behaviors of U-shaped ECC/RC composite beams are conducted in this paper. Two counterpart RC beams and six composite beams with different formwork surface treatment were tested in bending. The load-deflection responses of the U-shaped ECC/RC composite beams were predicted by the strip method, while the flexural capacity of the composite beam is calculated by a simplified method. According to the experimental observation and theoretical results, the following conclusions can be drawn.

1) Hybrid PVA-ECC can achieve the strain hardening and steady-state multiple cracking behaviors under four-point bending test. Moreover, the hybrid PVA-ECC attains a compressive strength of approximately 43.5 MPa at a higher strain of 0.58%, with a gentle post-peak behavior due to fiber-bridging action.

2) All the specimens with U-shaped ECC formworks showed the ductile flexural failure instead of the debonding failure before the crushing of concrete, due to improvement in the interfacial resistance by increasing the interface area using the U-shaped formwork even with a smooth inner surface.

3) Unlike the flat plateau in the load-deflection curve of the RC beam, a softening behavior will be observed after peak load in U-shaped ECC/RC composite beams, which indicates that debonding between ECC and concrete has a

more significant effect on the load-carrying capacity than on the strain-hardening behavior of ECC.

4) The U-shaped ECC/RC composite beams achieve a larger yielding and ultimate load, as well as an improvement in deflection capacity due to the strain-hardening properties of the ECC matrix in formwork.

5) The surface condition in ECC/RC beams has little influence on the peak load, but it affects the ductility of the members. The surface with transverse grooves shows the best ductility because of the best interfacial bonding, followed by the surface with embedded sand particles and the smooth as-finished surface.

6) As expected, there are large numbers of fine cracks at the constant moment region of the composite beam rather than several wide cracks in the RC beams. Moreover, the crack width of the ECC in the formwork does not even exceed 100 μm when the applied load is less than 80% of the peak load, which can effectively enhance the structural durability.

7) A theoretical model based on the strip method was developed to predict the load-deflection response of ECC/RC composite beam. The calculated curve by the proposed model is shown to be consistent with the tested data to a certain extent.

8) A simplified method was evolved by the effective rectangular stress distribution approach to facilitate design of practical engineering, and good agreement has been obtained between the flexural capacities calculated by the simplified method and the fiber strip method as well as the experimental results.

Acknowledgements The authors acknowledge the funding supports of National Key Research and Development Plan, China (2016YFC0701400, 2017YFC1500700), and the National Natural Science Foundation of China (Grant No. 51778462).

References

1. Gergely P, Lutz L A. Maximum crack width in reinforced concrete flexural members. American Concrete Institute, 1973, 20: 87–117
2. Li V C, Leung C K Y. Steady state and multiple cracking of short random fiber composites. Journal of Engineering Mechanics, 1992, 118(11): 2246–2264
3. Li V C, Stang H, Krenchel H. Micromechanics of crack bridging in fiber reinforced concrete. Materials and Structures, 1993, 26(8): 486–494
4. Li V C, Mishra D K, Wu H C. Matrix design for pseudo-strain-hardening fibre reinforced cementitious composites. Materials and Structures, 1995, 28(10): 586–595
5. Li V C, Wu H C, Chan Y W. Effect of plasma treatment of polyethylene fibers on interface and ementitious composite properties. Journal of the American Ceramic Society, 1996, 79(3): 700–704
6. Li V C, Wang S, Wu C. Tensile strain-hardening behavior of polyvinyl alcohol engineered cementitious composite (PVA-ECC). ACI Materials Journal, 2001, 98(6): 483–492
7. Şahmaran M, Li V C, Li M. Transport properties of engineered cementitious composites under chloride exposure. ACI Materials Journal, 2007, 104: 604–611
8. Wang K, Jansen D, Shah S, Karr A. Permeability study of cracked concrete. Cement and Concrete Research, 1997, 27(3): 381–393
9. Lepech M D, Li V C. Long term durability performance of engineered cementitious composites. Restoration of Buildings and Monument, 2006, 12(2): 119–132
10. Wang S X, Li V C. Engineered cementitious composites with high-volume fly ash. ACI Materials Journal, 2007, 104(3): 233–241
11. Pan Z F, Wu C, Liu J Z, Wang W, Liu J W. Study on mechanical properties of cost-effective polyvinyl alcohol engineered cementitious composites (PVA-ECC). Structure and Building Material, 2015, 78(3): 397–404
12. Fischer G, Li VC. Influence of matrix ductility on tension stiffening behavior of steel reinforced engineered cementitious composites. ACI Structural Journal, 2002, 99(1): 104–111
13. Maalej M, Li V C. Introduction of strain hardening engineered cementitious composites in design of reinforced concrete flexural members for improved durability. ACI Structural Journal, 1995, 92(2): 167–176
14. Leung C K, Cao Q. Development of pseudo-ductile permanent formwork for durable concrete structures. Materials and Structures, 2010, 43(7): 993–1007
15. Yuan F, Pan J L, Leung C K Y. Flexural behaviors of ECC and concrete/ECC composite beams reinforced with basalt fiber-reinforced polymer. Journal of Composites for Construction, 2013, 17(5): 591–602
16. Li Q H, Xu S L. Experimental investigation and analysis on flexural performance of functionally graded composite beam crack-controlled by ultrahigh toughness cementitious composites. Science in China Series E: Technological Sciences, 2009, 52(6): 1648–1664
17. Yang E H, Yang Y, Li V C. Use of high volumes of fly ash to improve ECC mechanical properties and material greenness. ACI Materials Journal, 2007, 104(6): 620–628
18. Qian S Z, Li V C. Simplified inverse method for determining the tensile properties of strain hardening cementitious composites (SHCC). Journal of Advanced Concrete Technology, 2008, 6(2): 353–363
19. American Association of State Highway and Transportation Officials (AASHTO). AASHTO LRFD Bridge Design Specifications. 4th ed. Washington D. C.: AASHTO, 2007
20. Rashid M A, Mansur M A. Reinforced high-strength concrete beams in flexure. ACI Structural Journal, 2005, 102(3): 462–471
21. Lepech M, Li V C. Water permeability of cracked cementitious composites. In: Proceedings of the 11th International Conference on Fracture. CD ROM, 2005
22. Maalej M, Li V C. Flexural/tensile strength ratio in Engineered Cementitious Composites. Journal of Materials in Civil Engineering, 1994, 6(4): 513–528
23. Hognestad E, McHenry D, Hanson N W. Concrete stress distribution in ultimate strength design. Journal of the American

Concrete Institute, 1955, 27(4): 455–479
24. Rüsch H. Researches toward a general flexural theory for structural concrete. Journal of the American Concrete Institute, 1960, 57(1): 1–28
25. Wu Y F, Oehlers D J, Griffith M C. Rational definition of the flexural deformation capacity of RC column sections. Engineering Structures, 2004, 26(5): 641–650
26. ACI Committee 318. Building code requirements for structural concrete (ACI 318-14). American Concrete Institute, Farmington Hills, MI, 2014